# Quantum critical behavior in an antiferromagnetic heavy-fermion Kondo lattice system $(Ce_{1-x}La_x)_2Ir_3Ge_5$*

Rajwali Khan[1], Qianhui Mao(毛乾辉)[1], Hangdong Wang(王杭栋)[2], Jinhu Yang(杨金虎)[2], Jianhua Du(杜建华)[1], Binjie Xu(许彬杰)[1], Yuxing Zhou(周宇星)[1], Yannan Zhang(张燕楠)[1], Bing Chen(陈斌)[2], and Minghu Fang(方明虎)[1,3,†]

[1] *Department of Physics, Zhejiang University, Hangzhou* 310027, *China*
[2] *Department of Physics, Hangzhou Normal University, Hangzhou* 310036, *China*
[3] *Collaborative Innovation Center of Advanced Microstructures, Nanjing* 210093, *China*

(Received 22 August 2016; revised manuscript received 28 September 2016; published online 30 November 2016)

The measurements on temperature dependences of magnetic susceptibility $\chi(T)$, specific heat $C(T)$, and electrical resistivity $\rho(T)$ were carried out for the antiferromagnetic (AFM) $(Ce_{1-x}La_x)_2Ir_3Ge_5$ $(0 \le x \le 0.66)$ system. It was found that the Neel temperature $T_N$ decreases with increasing La content $x$, and reaches 0 K near a critical content $x_{cr} = 0.6$. A new phase diagram was constructed based on these measurements. A non-Fermi liquid behavior in $\rho(T)$ and a $\log T$ relationship in $C(T)$ were found in the samples near $x_{cr}$, indicating them to be near an AFM quantum critical point (QCP) with strong spin fluctuation. Our finding indicates that $(Ce_{1-x}La_x)_2Ir_3Ge_5$ may be a new platform to search for unconventional superconductivity.

**Keywords:** quantum critical point, antiferromagnetic Kondo lattice system, $(Ce_{1-x}La_x)_2Ir_3Ge_5$

**PACS:** 74.40.kb, 75.50.Ee, 74.25.F–, 75.20.Hr **DOI:** 10.1088/1674-1056/26/1/017401

## 1. Introduction

Quantum criticality has become one of the most fascinating subjects in condensed matter physics for the last two decades. As a system reaches a certain threshold point, quantum fluctuations at 0 K are so strong that the metallic state of the system is broken. Quantum critical fluctuations are the strongest disturbances that can be exerted on the metallic state, which are the top candidates to explain the mysterious behaviors of heavy fermions,[1,2] high-temperature superconductivity in cuprates,[3,4] and doped ferromagnetic and antiferromagnetic (AFM) systems.[1,5] Heavy-fermion compounds have played the key role in the study of the AFM quantum critical behavior. Recently, AFM Kondo-lattice systems have been tuned to the quantum critical point (QCP) by modifying the external parameters, such as the magnetic field, pressure, and chemical doping,[6] and many exotic quantum phenomena have been found near QCP. In $CeCoIn_5$,[7–9] $CeCu_{5.2}Ag_{0.8}$,[10] and $YbRh_2Si_2$,[11,12] AFM QCP can be realized by modifying the magnetic field. While in $CeRh_2Si_2$,[13] $CeCu_2Ge_2$,[14] $CeIn_3$, and $CePd_2Si_2$[15] systems, the Neel temperature $T_N$ can be driven to 0 K by an external applied pressure. There are a few examples for the realization of AFM QCP by chemical substitution in the Ce-based heavy-fermion Kondo lattice systems, such as in $Ce(Cu_{1-x}Au_x)_6$ $(x = 0.1)$[16] and $(CeIn_{3-x}Sn_x)$,[17] which are close to AFM QCP.

$Ce_2Ir_3Ge_5$ is an AFM Kondo-lattice system with Neel temperature $T_N = 9.5$ K.[18] It crystallizes in the tetragonal ($U_2Co_3Si_5$) structure (*Ibam*). While $La_2Ir_3Ge_5$ is a non magnetic compound,[19] which crystallizes in the same structure as that of $Ce_2Ir_3Ge_5$. Yuan and his coworkers[20] found that the magnetic order in $Ce_2Ir_3Ge_5$ can be easily suppressed by applying a hydrostatic pressure. Here we show that the AFM order can be suppressed by the partial substitution of La for Ce in the $(Ce_{1-x}La_x)_2Ir_3Ge_5$ system. It is found that the $T_N$ decreases with increasing La content and reaches 0 K near a critical content $x_{cr} = 0.6$. A new phase diagram is constructed based on our measurements for this system. The non-Fermi liquid behavior in $\rho(T)$ and the $\log T$ relationship in $C(T)$ of the samples near $x_{cr}$ demonstrate that strong spin fluctuation emerges in these samples, indicating them to be near AFM QCP.

## 2. Experimental method

Polycrystalline samples of the solid solutions $(Ce_{1-x}La_x)_2Ir_3Ge_5$ $(0 \le x \le 0.66)$ were prepared by a conventional arc-melting method. The starting materials were cut from pieces of Ce (Alfa Aesar, 99.9%), La (Alfa Aesar, 99.9%), Ir (Alfa Aesar, 99.9%), and Ge (Alfa Aesar Puratronic, 99.9999%). After melting, each sample was flipped over and re-melted several times for homogeneity. The resulting samples were sealed inside evacuated quartz tubes and annealed at 930 °C for one week. It was found that the net

*Project supported by the National Basic Research Program of China (Grant Nos. 2016FYA0300402, 2015CB921004, and 2012CB821404) and the National Natural Science Foundation of China (Grant Nos. 11374261 and 11204059).

†Corresponding author. E-mail: mhfang@zju.edu.cn

 

weight loss was less than 1% for each sample during these processes. Powder x-ray diffraction patterns for all the samples were recorded at room temperature by a PANalytical x-ray diffractometer (Model EMPYREAN) with monochromatic Cu $K\alpha_1$ radiations. Analysis of the x-ray powder-diffraction data was made by using the High ScorePlus software. The DC magnetic susceptibility was measured at a magnetic field of 1000 Oe using a Quantum Design MPMS (SQUID). The heat capacity and resistivity measurements were carried out by using a Quantum Design physical properties measurement system (PPMS).

## 3. Results and discussion

Figure 1(a) shows the powder x-ray diffraction (XRD) pattern of the un-doped $Ce_2Ir_3Ge_5$ sample, together with its Rietveld refinement (weighted profile factor $R_{WP} = 2.35\%$ and the goodness-of-fit $\chi^2 = 1.58$). All the peaks can be indexed by a $U_2Co_3Si_5$ orthorhombic structure,[21] with a space group of *Ibam*. Figure 1(b) shows the XRD patterns of the $(Ce_{1-x}La_x)_2Ir_3Ge_5$ ($x = 0.1$, 0.3, and 0.6) samples, indicating that all the samples ($0 \le x \le 0.66$) are a single phase. The lattice parameters were obtained by fitting the XRD data, as shown in Figs. 1(c)–1(e). For example, for the pure $Ce_2Ir_3Ge_5$ ($x = 0.0$) sample, $a = 10.198(1)$ Å, $b = 11.938(1)$ Å, and $c = 6.069(1)$ Å, which are the same as those reported by Hossain *et al.*[18] With increasing La content $x$, the lattice parameters $a$, $b$, and $c$ increase monotonically, which is consistent with the fact that the ionic radius of $La^{3+}$ (1.061 Å) is larger than that of $Ce^{3+}$ (1.034 Å). These results demonstrate that $La^{3+}$ can uniformly substitute for $Ce^{3+}$ in the $(Ce_{1-x}La_x)_2Ir_3Ge_5$ ($0 \le x \le 0.66$) system.

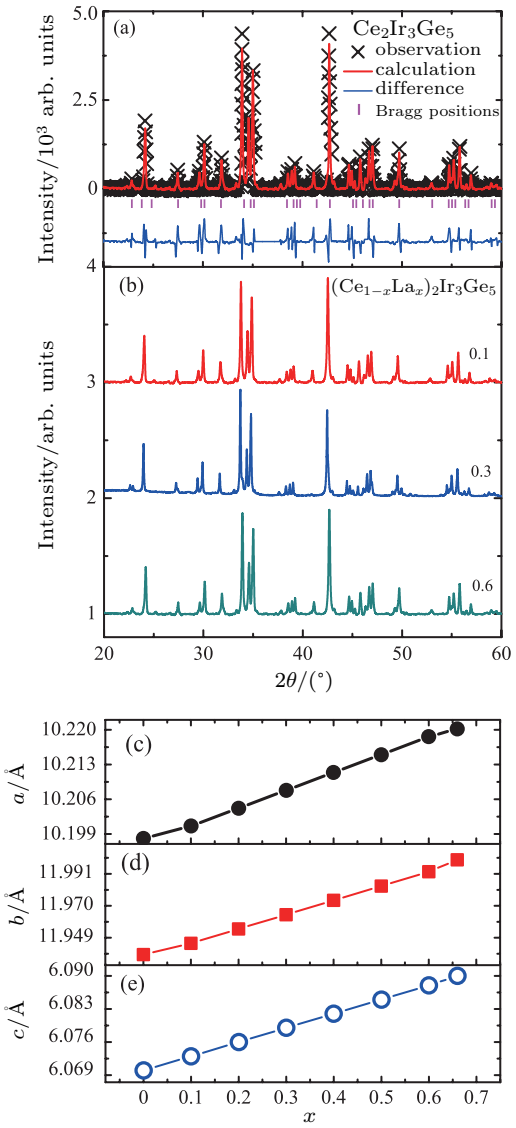


**Fig. 1.** (color online) (a) X-ray diffraction patten of $Ce_2Ir_3Ge_5$ and its Rietveld refinement. (b) Powder XRD patterns of $(Ce_{1-x}La_x)_2Ir_3Ge_5$ ($x = 0.1$, 0.3, and 0.6) samples. Lattice parameters (c) $a$, (d) $b$, and (e) $c$ as functions of the La content $x$ for $(Ce_{1-x}La_x)_2Ir_3Ge_5$ ($0 \le x \le 0.66$).

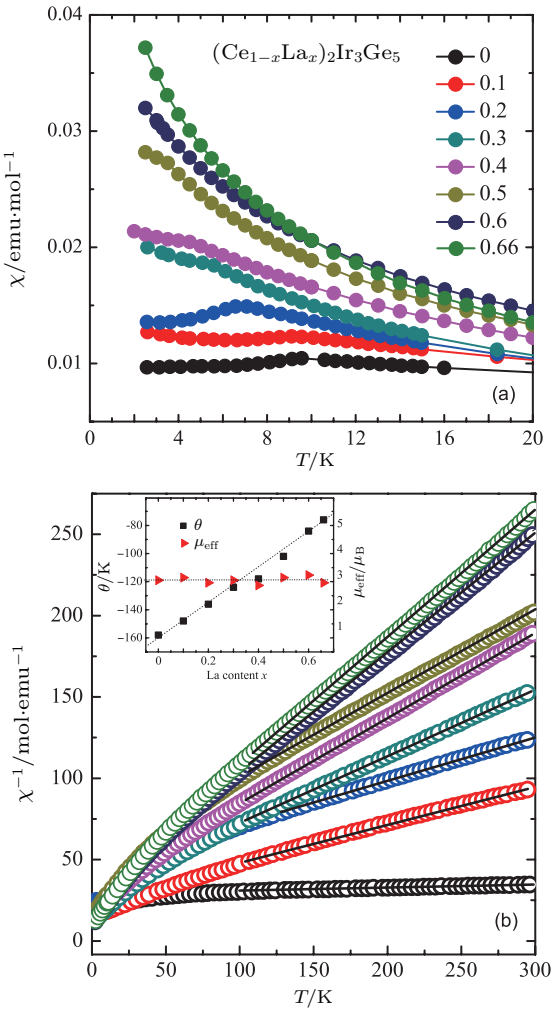


**Fig. 2.** (color online) (a) Temperature dependence of magnetic susceptibility, $\chi(T)$, for $(Ce_{1-x}La_x)_2Ir_3Ge_5$ ($0 \le x \le 0.66$), under an applied magnetic field of 1000 Oe. (b) The inverse susceptibility fitted with the Curie–Weiss law for $(Ce_{1-x}La_x)_2Ir_3Ge_5$ ($0 \le x \le 0.66$). The inset shows effective moment $\mu_{eff}$ and Curie–Weiss temperature $\theta$ for the $0 \le x \le 0.66$ samples.

Figure 2(a) shows the temperature dependence of the magnetic susceptibility, $\chi(T)$, for the $(Ce_{1-x}La_x)_2Ir_3Ge_5$ ($0 \le x \le 0.66$) samples below 20 K in a magnetic field of 1000 Oe.

For the pure $Ce_2Ir_3Ge_5$ sample, the AFM transition is characterized by a little decrease in $\chi(T)$ at Neel temperature $T_N = 9.5$ K as reported by Hossain *et al.*[18] With increasing La content, $T_N$ decreases and becomes invisible for $x_{cr} = 0.60$. A similar behavior has been discovered in $Ce_2Ir_3Ge_5$ under an external pressure.[20] Figure 2(b) displays the temperature dependence of the inverse magnetic susceptibility, $\chi^{-1}(T)$, for the $(Ce_{1-x}La_x)_2Ir_3Ge_5$ ($0 \le x \le 0.66$) samples. It is clear that the $\chi^{-1}(T)$ curves exhibit a linear behavior above 100 K. To fit the $\chi(T)$ data above 100 K, we used the modified Curie–Weiss law[18]

$$\chi = \chi_0 + C/(T-\theta), \tag{1}$$

where $\chi_0$ represents the temperature-independent susceptibility, $C$ is the Curie constant, and $\theta$ is the Curie–Weiss temperature. For the pure $Ce_2Ir_3Ge_5$ ($x = 0.0$) sample, the effective moment $\mu_{eff} = 2.8\ \mu_B$ was estimated by this fitting, which is close to that for a free $Ce^{3+}$ ion (2.54 $\mu_B$). It was also found that the effective moment $\mu_{eff} \sim 2.83\ \mu_B$ for all the $(Ce_{1-x}La_x)_2Ir_3Ge_5$ ($0 \le x \le 0.66$) samples is almost independent of the La content, as shown in the inset of Fig. 2(b), indicating that there is no effect on the delocalization of the 4f electron from the partial substitution of La for Ce. The negative Curie–Weiss temperature, $\theta = -158$ K for the $x = 0.0$ sample, indicates the presence of the Kondo interaction. As shown in the inset of Fig. 2(b), it is clear that $\theta$ increases with increasing La content, from $-158$ K ($x = 0.0$) to $-78$ K ($x = 0.66$), which is related to the Ruderman–Kittel–Kasuya–Yoshida (RKKY) coupling. It is clear that the distance between the Ce-ions increases with the La doping, then the RKKY coupling becomes weaker, as discussed by Lora-Serrano *et al.* for $Nd_{1-x}La_xRhIn_5$.[22]

Figure 3(a) shows the temperature dependence of the resistivity, $\rho(T)$, for the $(Ce_{1-x}La_x)_2Ir_3Ge_5$ ($0 \le x \le 0.66$) samples. The $\rho(T)$ curves for the $x \le 0.5$ samples show a typical behavior of the AFM Kondo-lattice system. For the pure $Ce_2Ir_3Ge_5$ ($x = 0.0$) sample, with decreasing temperature, the resistivity decreases monotonously to $\sim 240\ \mu\Omega$·cm at 9.5 K, then drops sharply to $\sim 34\ \mu\Omega$·cm at 2 K, which is associated with the AFM transition. For the $(Ce_{1-x}La_x)_2Ir_3Ge_5$ ($0.1 \le x \le 0.5$) samples, their resistivity decreases at first with decreasing temperature, reaches a minimum at about 38 K, then increases to a maximum, finally it drops sharply at $T_N$. In the paramagnetic state, the minimum in $\rho(T)$ originates from the existence of the Kondo effect in the sample as discussed by Gignoux *et al.*[24] As shown in Fig. 3(b), the Neel temperature $T_N$ decreases with increasing La content. Only for the $x = 0.6$ and 0.66 samples, their $\rho(T)$ exhibit a metallic behavior in the whole measuring temperature range (2–300 K). In order to explore the evolution of the $\rho(T)$ behavior with the partial substitution of La for Ce, we first fitted the $\rho(T)$ data in the AFM state by using the following expression:[25,26]

$$\rho(T) = \rho_0 + AT^2 + BT\Delta(1+2T/\Delta)\,e^{-\Delta/T}, \tag{2}$$

where $\rho_0$ is the residual resistivity, $A$ is the coefficient of

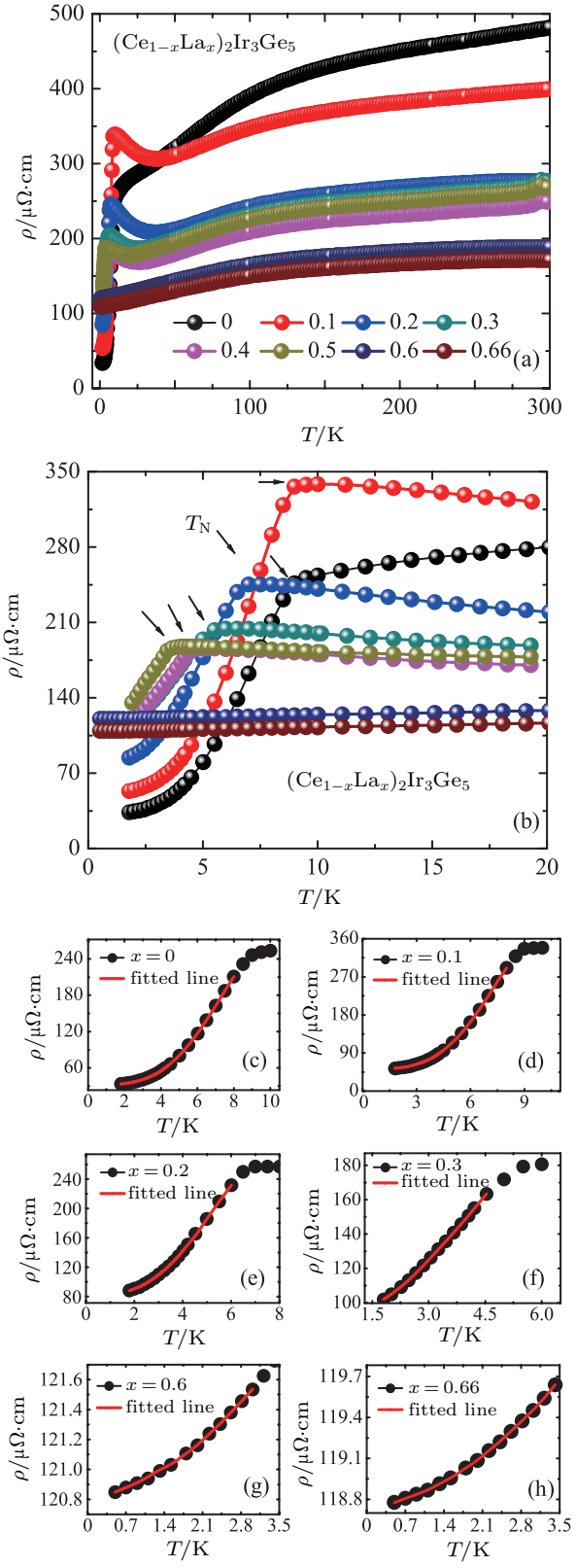


**Fig. 3.** (color online) (a) Temperature dependence of electrical resistivity in $(Ce_{1-x}La_x)_2Ir_3Ge_5$ ($0 \le x \le 0.66$). (b) Resistivity in the low-temperature range around $T_N$ (marked by an arrow). (c)–(h) $\rho(T)$ in the lower temperature range for $x = 0.0$, 0.1, 0.2, 0.3, 0.6, and 0.66 samples fitted by Eq. (2) or $\rho(T) = \rho_0 + A'T^n$, as discussed in the text.

the Fermi-liquid $T^2$ term, $B$ involves the electron–magnon scattering, and $\Delta$ is the magnitude of the gap. It is clear that $\rho(T)$ in the AFM state for all the $x \leq 0.5$ samples can be well described by Eq. (2), as shown in Figs. 3(c)–3(f). By this fitting, we obtained $\rho_0 = 34$ μΩ·cm, 58 μΩ·cm, 85 μΩ·cm, 98 μΩ·cm, 116 μΩ·cm, and 119 μΩ·cm and $A =$ 1.8 μΩ·cm/K$^2$, 2.1 μΩ·cm/K$^2$, 2.7 μΩ·cm/K$^2$, 3.5 μΩ·cm/K$^2$, 4.1 μΩ·cm/K$^2$, and 4.9 μΩ·cm/K$^2$ for the $x = 0.0$, 0.1, 0.2, 0.3, 0.4, and 0.5 samples, respectively. Both the $\rho_0$ and $A$ values increase with increasing La content. The energy gap $\Delta$ decreases from $\Delta = 35$ K for $x = 0.0$ to $\Delta = 15$ K for $x = 0.5$. On the other hand, for the $x = 0.6$ and 0.66 samples, their $\rho(T)$ cannot be described by either the Fermi-liquid behavior $\rho(T) = \rho_0 + AT^2$ or Eq. (2). Then we used a power law expression $\rho(T) = \rho_0 + A'T^n$ to fit the $\rho(T)$ data at lower temperatures for both samples, as shown in Figs. 3(g) and 3(h), where $A'$ is the temperature coefficient and $n$ is the power exponent. It was estimated that $n$ is 1.3 and 1.5 for the $x = 0.6$ and 0.66 samples, which is smaller than 2, indicating that their $\rho(T)$ deviate from the Fermi-liquid behavior. At the same time, we also found that both $\rho_0$ and $A$ values reach a maximum for the $x = 0.6$ sample (see Figs. 5(b) and 5(d)).

Figure 4(a) shows the temperature dependence of the heat capacity, $C(T)$, for the $(Ce_{1-x}La_x)_2Ir_3Ge_5$ ($0 \leq x \leq 0.66$) samples. It is clear that a $\lambda$-type anomaly in $C(T)$ corresponding to the AFM transition emerges at $T_N$ for the $(Ce_{1-x}La_x)_2Ir_3Ge_5$ ($0 \leq x \leq 0.5$) samples, and $T_N$ decreases with increasing La content. For the $x = 0.6$ and 0.66 samples, no $\lambda$-type anomaly in $C(T)$ is observed above 0.5 K. In order to obtain more information from the $C(T)$ data, we re-plotted the $C(T)$ data as $C/T$ vs. $\log T$ in Fig. 4(b). First we analyze the $C(T)$ data in the AFM state for the $(Ce_{1-x}La_x)_2Ir_3Ge_5$ ($0 \leq x \leq 0.5$) samples. As discussed by Coqblin *et al.*,[27] $C(T)$ should be described by the expression

$$C(T) = \gamma_0 T + \beta T^3 + \alpha(\Delta^2/\sqrt{T} + 3\Delta\sqrt{T} + 5\sqrt{T^3})\,e^{-\Delta/T}, \quad (3)$$

where the first term represents the specific heat from the electrons, the second term is the contribution from the lattice vibration, and the third term represents the contribution of the magnons with a gap. For clarity, figure 4(b) only shows the fitting line (red) below 9 K for the $Ce_2Ir_3Ge_5$ sample. In fact, the $C(T)$ data below $T_N$ for all the $x \leq 0.4$ samples can be well described by Eq. (3). Table 1 lists the electronic specific heat coefficient $\gamma_0$, the lattice specific heat coefficient $\beta$, the magnon specific heat coefficient $\alpha$, and the corresponding gap $\Delta$ for the $x = 0.0$, 0.1, 0.2, 0.3, and 0.4 samples. It is obvious that $\gamma_0$ increases while $\alpha$ and $\Delta$ decrease with increasing La content, indicating that the partial substitution of La for Ce results in the enhancement of the electronic specific heat and the reduction in the magnon specific heat. However, the specific heat $C(T)$ below 9 K for the $x = 0.6$ and 0.66 samples, in which the AFM order disappears, exhibits a $\log T$ behavior. We used the expression[28,29]

$$C/T = \gamma_0 + \beta T^2 + \delta \log(T_0/T) \quad (4)$$

to fit the $C(T)$ data for both $x = 0.6$ and 0.66 samples, where $\delta$ is a coefficient and $T_0$ presents a characteristic temperature related to the spin fluctuation term. For clarity, figure 4(b) only shows the fitting (yellow) line for the $x = 0.66$ sample. The fitting parameters for both $x = 0.6$ and 0.66 samples to Eq. (4) are listed in Table 2. From the results listed in Tables 1 and 2, it can be concluded that the electronic specific heat coefficient $\gamma_0$ increases with increasing La content and reaches a maximum 101.1 mJ/mol·K$^2$ in the $x = 0.6$ sample, then drops a little in the $x = 0.66$ sample. Especially, the $C/T \sim \log T$ behavior emerges in the $x = 0.6$ and 0.66 samples, which is a typical behavior for the system with strong spin fluctuation,[30,31] indicating that the $x = 0.6$ sample is located near AFM QCP. No obvious change in $\beta$ was found for all the samples, indicating that the partial substitution of La for Ce has little influence on their Debye temperature. For example, by using the fitted $\beta$ values in the Debye expression $\Theta_D = [(12/5)NR\pi^4/\beta]^{1/3}$, the Debye temperature $\Theta_D$ was estimated to be 240 K, 238 K, and 242 K for the $x = 0.0$, 0.3, and 0.6 samples, respectively.

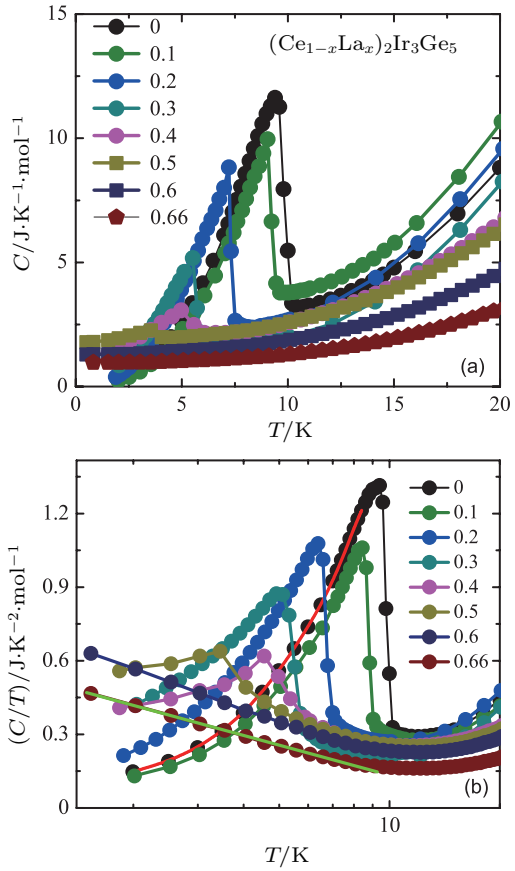


**Fig. 4.** (color online) (a) Temperature dependence of specific heat $C(T)$ and (b) $C/T$ as a function of $\log T$ for the $(Ce_{1-x}La_x)_2Ir_3Ge_5$ ($0 \leq x \leq 0.66$) samples. Red line: fitting to the $C(T)$ data of the $x = 0.0$ sample by Eq. (3), deep yellow line: fitting to the $C(T)$ data of the $x = 0.66$ sample by Eq. (4).

**Table 1.** Fitting parameters $\gamma_0$, $\beta$, $\alpha$, and $\Delta$ of the $C(T)$ data below $T_N$ for the $0 \le x \le 0.4$ samples with Eq. (3).

| $x$ | $\gamma_0$/mJ·mol$^{-1}$·K$^{-2}$ | $\beta$/mJ·mol$^{-1}$·K$^{-4}$ | $\alpha$/J·mol$^{-1}$·K$^{-5/2}$ | $\Delta$/K |
|---|---|---|---|---|
| 0.0 | 69.2 | 1.401 | 0.240 | 32 |
| 0.1 | 72.4 | 1.312 | 0.215 | 30 |
| 0.2 | 78.1 | 1.351 | 0.191 | 28 |
| 0.3 | 82.7 | 1.425 | 0.175 | 27 |
| 0.4 | 90.2 | 1.632 | 0.159 | 24 |

**Table 2.** Fitting parameters $\gamma_0$, $\beta$, $\delta$, and $T_0$ of the $C(T)$ data in the low temperature range for the $x = 0.6$ and 0.66 samples with Eq. (4).

| $x$ | $\gamma_0$/mJ·mol$^{-1}$·K$^{-2}$ | $\beta$/mJ·mol$^{-1}$·K$^{-4}$ | $\delta$/mJ·mol$^{-1}$·K$^{-1}$ | $T_0$/K |
|---|---|---|---|---|
| 0.6 | 101.1 | 1.352 | 0.151 | 34 |
| 0.66 | 94.8 | 1.535 | 0.125 | 18 |

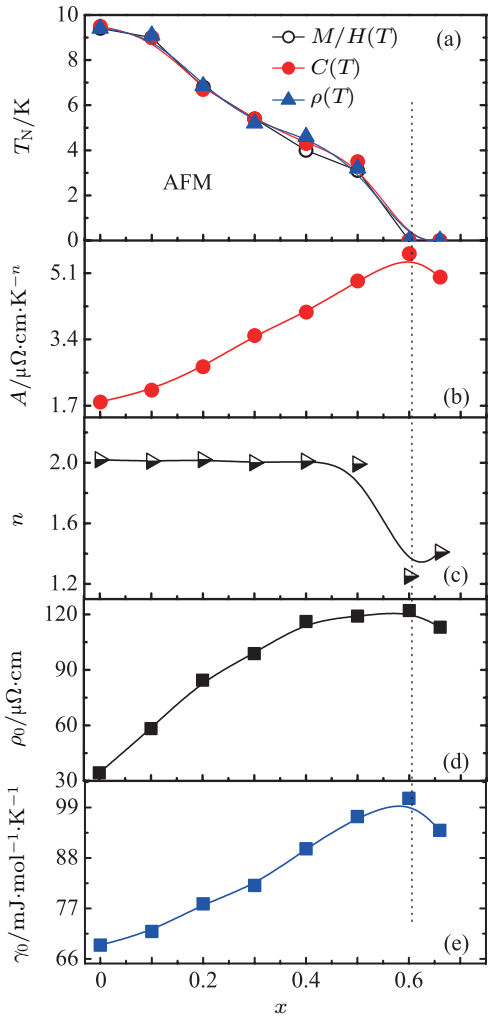


**Fig. 5.** (color online) La concentration $x$ dependence of (a) AFM Neel temperature $T_N$ as estimated from the $\chi(T)$, $C(T)$, and $\rho(T)$ of $(Ce_{1-x}La_x)_2Ir_3Ge_5$ ($0 \le x \le 0.66$), (b) the temperature coefficient $A$, (c) the power exponent $n$, (d) the residual resistivity $\rho_0$, which are the fitting parameters to $\rho(T)$, see the text. (e) The electronic specific heat coefficient $\gamma_0$ obtained from the $C(T)$ data, as discussed in the text.

Based on the results of $\rho(T)$, $\chi(T)$, and $C(T)$ measurements, we constructed the phase diagram of Néel-temperature $T_N$ as a function of La content $x$ for the $(Ce_{1-x}La_x)_2Ir_3Ge_5$ system, as shown in Fig. 5(a). With increasing La content, $T_N$ decreases and reaches 0 K at a critical content $x_{cr} = 0.6$. Figures 5(b)–5(e) show the $A$ ($A'$), $n$, $\rho_0$, and $\gamma_0$ as functions of La content $x$. It is obvious that all the fitting parameters with Eq. (2)–(4) and the $\rho(T)$ power law exhibit an anomalous near $x_{cr}$. For example, the power exponent $n = 2$ in the $0 \le x \le 0.5$ samples, indicating that the Fermi-liquid behavior occurs in this region, i.e., there are two kinds of electrons: itinerant and localized ones. Whereas for the $x = 0.6$ and 0.66 samples, $n$ is less than 2.0, and reaches a minimum of 1.3 in the $x_{cr} = 0.6$ sample, signaling that a non-Fermi liquid behavior emerges in these samples (see Fig. 5(c)). All the $A$, $\rho_0$, and $\gamma_0$ values reach to maximum at $x_{cr}$, as shown in Figs. 5(b), 5(d), and 5(e), respectively. All the anomalous in $n$, $A$, $\rho_0$, and $\gamma_0$ at $x_{cr}$, in addition to the $C/T \sim \log(T_0/T)$ behavior near $x_{cr}$, indicate that a strong spin-fluctuation emerges in the samples near $x_{cr}$, which is similar to that in the doping induced AFM QCP $UCo_{1-x}Fe_xGe$[32] and $YbNi_2(P_{1-x}As_x)_2$[33] systems. Our finding implies that $(Ce_{1-x}La_x)_2Ir_3Ge_5$ may provide another platform to study AFM quantum fluctuation near QCP. We are looking forward to finding some exotic quantum states, such as superconductivity after obtaining a high quality single crystal in the future.

## 4. Conclusion

We synthesized successfully AFM $(Ce_{1-x}La_x)_2Ir_3Ge_5$ ($0 \le x \le 0.66$) heavy-fermion alloys. Based on the measurements of magnetization, resistivity, and specific heat, the magnetic phase diagram was obtained for this system. It was found that the Neel temperature $T_N$ decreases with increasing La content $x$, and reaches 0 K near $x_{cr} = 0.6$. The non-Fermi liquid behavior in $\rho(T)$ and the $C(T)/T \propto \log T$ relationship in the samples near $x_{cr}$ demonstrate that an AFM quantum phase transition occurs at $x_{cr}$. These results imply that $(Ce_{1-x}La_x)_2Ir_3Ge_5$ provides a platform for searching for the new exotic collective phases, such as unconventional superconductivity.

## References


[1] Lohneysen H V, Rosch A, Vojta M and Wolfle P 2007 *Rev. Mod. Phys.* **79** 1015

[2] Coleman P, Pepin C, Si Q and Ramazashvili R 2001 *J. Phys.: Condens. Matter* **13** R723

[3] Lee P A, Nagaosa N and Wen X G 2006 *Rev. Mod. Phys.* **78** 17

[4] Norman M R and Pepin C 2003 *Rev. Mod. Phys.* **66** 1547

[5] Rost A W, Grigera S A, Bruin J A N, *et al.* 2011 *Proc. Natl. Acad. Sci. USA* **180** 16549

[6] Dhar S K, Kulkarni R, Hidaka H, Toda Y, Kotegawa H, Kobayashi T C, Manfrinetti P and Provino A 2009 *J. Phys.: Condens. Matter* **21** 156001

[7] Wang C H, Poudel L, Taylor A E, Lawrence J M, Christianson A D, Chang S, Rodriguez-Rivera J A, Lynn J W, Podlesnyak A A, Ehlers G, Baumbach R E, Bauer E D, Gofryk K, Ronning F, McClellan K J and Thompson J D 2015 *J. Phys.: Condens. Matter* **27** 015602

[8] Bianchi A, Movshovich R, Vekhter I, Pagliuso P G and Sarrao J L 2003 *Phys. Rev. Lett.* **91** 257001

[9] Paglione J, Tanatar M A, Hawthorn D G, Boaknin E, Hill R W, Ronning F, Sutherland M, Taillefer L, Petrovic C and Canfield P C 2003 *Phys. Rev. Lett.* **91** 246405
[10] Heuser K, Kim J S, Scheidt E W, Schreiner T and Stewart G R 1999 *Physica B* **259** 392
[11] Gegenwart P, Custers J, Geibel C, Neumaier K, Tayama T, Tenya K, Trovarelli O and Steglich F 2002 *Phys. Rev. Lett.* **89** 056402
[12] Ishida K, Okamoto K, Kawasaki Yu, Kitaoka Y, Trovarelli O and C Geibel C 2003 *Phys. Rev. Lett.* **89** 107202
[13] Movshovich R, Graf T, Mandrus D, Thompson J D, Smith J L and Fisk Z 1996 *Phys. Rev. B* **52** 8241
[14] Jaccard D, Behnia K and Sierro J 1992 *Phys. Lett. A* **163** 475
[15] Mathur N D, Grosche F M, Julian S R, Walker I R, Freye D M, Haselwimmer R K W and Lon-zarich G G 1998 *Nature* **394** 39
[16] Lohneysen H V, Pietrus T, Portisch G, Schlager H G, Schroder A, Sieck M and Trappmann T 2001 *Phys. Rev. Lett.* **72** 3262
[17] Kuchler R, Gegenwart P, Custers J, Stockert O, Caroca-Canales N, Geibel C, Sereni J G and Steglich F 2006 *Phys. Rev. Lett.* **96** 256403
[18] Hossain Z, Ohmoto H, Umeo K, Iga F, Suzuki T, Takabatake T, Takamoto N and Kindo K 1999 *Phys. Rev. B* **60** 10383
[19] Singh Y and Ramakrishnan S 2004 *Phys. Rev. B* **69** 174423
[20] Yuan H Q, Hossaina Z, Groschea F M, Sparn G, Geibela C, Steglicha F and Gupta L C 2002 *Physica B* **312** 187
[21] Venturini G, Meot-Meyer M, Marcche J F, Malaman B and Roques B 1986 *Mater. Res. Bull* **21** 33
[22] Lora-Serrano R, Garcia D J, Miranda E, Adriano C, Bufaical L, Duque J G S and Pagliuso P G 2009 *Physica B* **404** 3059
[23] Cornut B and Coqblin B 1972 *Phys. Rev. B* **5** 4541
[24] Gignoux D, Schmidt D, Zerguine M, Bauer E, Pillmayer N, Henry J Y, Nguyen V N and Rossat Mignod J 1988 *J. Magn. Magn. Mater.* **74** 1
[25] Sidorov V A, Bauer E D, Frederick N A, Jeffries J R, Nakatsuji S, Moreno N O, Thompson J D, Maple M B and Fisk Z 2003 *Phys. Rev. B* **67** 224419
[26] Inamdar M, Thamizhavel A and Dhar S K 2014 *J. Phys.: Condens. Matter* **26** 326003
[27] Coqblin B 1977 *The Electronic Structure of Rare-earth Metals and Alloys: the Magnetic Heavy Rare-earths* (New York: Academic) p. 211
[28] Stochert O, Lohneysen H V, Rosch A, Pyka N and Loewenhaupt M 1998 *Phys. Rev. Lett.* **80** 5627
[29] Nickla M, Brando M, Knebel G, Mayr F, Trinkl W and Loidl A 1999 *Phys. Rev. Lett.* **82** 4268
[30] Kittler W, Fritsch V, Weber F, Fischer G, Lamago D, Andre G and Lohneysen H V 2013 *Phys. Rev. B* **88** 165123
[31] Stewart G R 2001 *Rev. Mod. Phys.* **73** 797
[32] Huang K, Hamlin J J, Baumbach R E, Janoschek M, Kanchanavatee N, Zocco D A, Ronning F and Maple M B 2013 *Phys. Rev. B* **87** 054513
[33] Steppke A, Kuuchler R, Lausberg S, Lengye E, Steinke L, Borth R, Luhmann T, Krellner C, Nicklas M, Geibel C, Steglich F and Brando M 2013 *Science* **1** 339